Article:

Begum, H., Xue, Y., Bolton, J.S. et al. (1 more author) (2022) The acoustical absorption by air-saturated aerogel powders. The Journal of the Acoustical Society of America, 151 (3). pp. 1502-1515. ISSN 0001-4966

https://doi.org/10.1121/10.0009635

The acoustical properties of air-saturated aerogel powders

H. Begum[1], Y. Xue[2], J. S. Bolton[3], K. V. Horoshenkov[1]

[1] *Department of Mechanical Engineering, The University of Sheffield, S1 3JD, United Kingdom*

[2] *Midea Corporate Research Center, Foshan, Guangdong, China, 528311*

[3] *Ray W. Herrick Laboratories, School of Mechanical Engineering, Purdue University, 177 S. Russell St., West Lafayette, Indiana 47907-2099, USA*

Abstract

The acoustical behavior of air-saturated aerogel powders in the audible frequency range is not well understood. It is not clear, for example, which physical processes control the acoustic absorption and/or attenuation in a very light, loose granular mix in which the grain diameter is on the order of a micron. The novelty of this work is the use of a Biot-type poro-elastic model to fit accurately the measured absorption coefficients of two aerogel powders with particle diameters in the range 1 – 40 μm. It is shown that these materials behave like a viscoelastic layer and their absorption coefficient depends strongly on the root mean square pressure in the incident wave. Further, it was found that the loss factor controlling the energy dissipation due to vibration of the elastic frame is a key model parameter. The value of this parameter decreased progressively with both frequency and sound pressure. In contrast, other parameters in the Biot-type poro-elastic model, e.g., the stiffness of the elastic frame and pore size, were found relatively independent of the frequency and amplitude of the incident wave. It is shown that these materials can be very efficient resonant absorbers in the low frequency range.

PACS: 43.20 Mv, 43.20 Ye, 43.55 Ev, 43.58 Bh

Keywords: Acoustics, aerogels, modelling, particles, porous materials

I. Introduction

The desire to develop a diverse class of lightweight, porous, and cost-effective materials for acoustic applications has been the focus of industrialists for the past few decades[1]. Traditionally, a large selection of these materials were fibrous layers and reticulated foams[2]. Companies are invested in the use of foams or fibrous materials due to their high percentage of open pore availability (e.g., section 13.9 in 2) and their versatile nature which makes it possible to incorporate them in the form of layered composites. Their porous nature allows them to be effective absorbers that can dissipate the acoustic energy of propagating sound waves, and some may have viscoelastic properties which control structure-borne noise by attenuating structural vibrations through near-field damping (NFD)[3], which is achieved *via* viscous interaction between the porous medium and the evanescent acoustical near-field of the vibrating structure. There may be additional dissipation due to the elastic nature of the frame if it is sufficiently stiff, i.e., when using poro-elastic media instead of limp porous media as near-field dampers[4]. The acoustical damping multifunctionality of porous media has been investigated for several years, and the study is summarized in Ref. 5, which also provides the theoretical fundamentals of the study introduced in this article. The most important macroscopic physical characteristics (also referred to as bulk properties) that determine the acoustical properties of foams and fibrous media are: (i) airflow resistivity/effective pore size; (ii) porosity; (iii) pore tortuosity; and (iv) elastic modulus of the frame[6]**.** Granular media are also of popular interest because of their useful sound absorption and sound insulating properties[7,8]. Materials like flint particles[9], hemp[10] and expanded clays[11,12] have already been extensively studied. In particular, classical acoustics theory like the Biot theory for poro-elastic media has proven to be capable of modeling sound absorption and insulation resulting from granular media that have complex and hierarchical micro-structures such as the granular activated carbon stacks[13].

Granular aerogels are gaining more interest as an acoustic product due to their unique microstructural properties, i.e., porosities of approximately 95%, very low bulk densities (e.g., 0.0120 g/cm^3) and large surface area values in the range from 700 to 900 m^2/g[14]. The global aerogel market was evaluated at 701 million USD in 2019 and is projected to reach 1395.5 million USD by 2027 with a reported compound annual growth rate (CAGR) of 9.3 percent. Its primary development is in the building, oil, and gas industries. Because of their chemical inertness and low thermal conductivity, aerogels are sought after products for pipe insulation and protection[15]. The main drawbacks, however, are their high-cost production (specifically for monolithic aerogels) and ever-changing economic barriers[16]. Nonetheless, their exciting acoustical properties still create the potential for profitable gain for industries. Sound waves have been observed to propagate through silica aerogels at one-third the speed of sound in air or less: i.e., at about 100 m/s[17]. Forest et al.[18] have also found that sound velocities in aerogels as low as 60 to 70 m/s. The latter property results in rather high acoustic attenuation in aerogels since it effectively increases a given layer depth at a fraction of a wavelength.

In general, there is a lack of combined experimental data and analytical models that are available to predict the acoustical properties of granular aerogels. There is some literature by Begum et al.[19] which focus on analytical models and experimental data of the acoustical properties of granular silica aerogels. However, that work was performed using material having millimetric grain sizes, and by using a triple porosity model where only pore size and particle size were taken into consideration, and not the elastic properties of the material frame. Xue, et al.[20] have observed non-linear acoustical behavior of aerogel particle stacks consisting of relatively small particles (i.e., 2 to 40 micron), the non-linearity being dependent on both frequency and depth of the sample stack. Further evidence of non-linearity is presented in this article. A majority of other research exclusively focuses on much denser granular media with millimetric grain mixes, e.g., Horoshenkov and Swift[21].

Earlier research by Song and Bolton[22] was directed at using a four-microphone standing wave tube and the transfer matrix method to determine fundamental acoustical properties such as wave number and characteristic impedance of limp or rigid porous materials: i.e., materials that can be modeled as effective fluids. Based on that information arbitrarily shaped porous material domains can then be modelled by providing data such as complex density and complex sound speed to finite element models, for example. In contrast, here the two-microphone standing wave tube method was used to measure the normal incidence absorption coefficients of aerogels layers[23], and the material was modeled as a poro-elastic layer, hence allowing for both frame and airborne waves within the aerogel layers[2].

Since a majority of literature has focused on millimetric[2,11] grain mixes with sub-millimeter pore sizes[24], there is a gap in the understanding of the acoustical behavior of powder aerogels whose particle sizes are close to a micron. Modelling such small particles with different excitation sound pressures will help us to understand the non-linear effects which typically develop in lightweight materials such as aerogels. Such an approach will also build the connection between the material's bulk properties, such as material density and particle size, and key acoustical characteristics such as the normal incidence absorption coefficient.

These were two primary motivations for the present work. Firstly, based on fitting the experimental data, the connections developed in that way can help to inversely characterize the aerogel's acoustical-related bulk properties, thus quantifying each bulk property's contribution to the material's sound absorption performance. Secondly, and consequently, it becomes possible to optimize the acoustical performance of this type of aerogel by designing or specifying these bulk properties appropriately.

The structure of this paper is as follows. In Section II, the experimental methods and characterization techniques used to measure the physical material properties of aerogel powders are described. Presented in Section III are the acoustical theories and the approach to modelling of the acoustics of aerogel granules. The results and related discussion are described in Section IV in which the data is interpreted with a mathematical model that can be used to characterize the acoustical related bulk properties. Concluding remarks, which summarize the characterization process and the main result are presented in Section V.

II. Materials and Methods

A. Materials Characterization

Microstructural observations of the particle size distribution of the silica aerogels studied here – Enova IC3100 produced by Cabot Corporation, Alpharetta Georgia, USA (denoted as Type 1), and JIOS AeroVa D20 produced by JIOS Aerogel, Korea (denoted as Type 2) were made by using scanning electron microscopy (SEM). The instrument used was an FEI Inspect F50 FEG SEM. The samples were mounted as per the manufacturer's guidelines and were initially carbon coated using a Quorum Technologies Q150T coater. However, that coating proved to be insufficient to prevent sample charging even at 5 kV, and therefore the samples were subsequently given a 5 nm gold coat using a Quorum Technologies Q150R gold sputter coater.

Secondary Electron Images (SE) were obtained at a range of accelerating voltages (kV) as indicated on the micrographs. Spot size 3 was used with the 20 μm final lens aperture (smallest for highest resolution) inserted. For the highest magnification images, the working distance (WD) was reduced to 6 mm from the standard 10 mm for Type 1.

Figures 1(a)–1(f) are SEM images of Type 1 and Type 2 aerogel powders. These images were used to identify the aerogel particle distribution and structure of the pore sizes. A Java-based image processing program, ImageJ, was used to manually measure the size of 100 individual Type 1 and Type 2 particles in images that were obtained at a high magnification (1000 x) at a scale bar of 100 μm. The data was collated to determine the normal approximation of the particle size distribution: see supplementary material in Ref. 25. The average Type 1 particle size was found to be 13.69 μm, with a minimum and maximum value of 7.91 μm and 24.83 μm, respectively, and the average Type 2 particle size was 14.20 μm with minimum and maximum values of 5.54 μm and 41.78 μm respectively. These average particle size values correspond to those which were used for the 3P-Biot-TMM/ACM modelling of the acoustical properties (detailed in Sections III and IV), and the measured minimum and maximum values of Type 1 and Type 2 aerogel powders also corresponded to the values given in the manufacturers' technical data sheets.

Note that the SEM magnification scale in each of the images in Figure 1 changes between 100 μm, 30 μm, 1 μm and 500 nm to provide a better insight into the particle microstructure. We note that SEM image analysis is sensitive to the detail of the loading of samples onto the carbon stub: i.e., when a large amount is deposited, the coating is affected, and this may fracture the image surfaces. Furthermore, there may be sampling bias causing the contrast/ brightness settings to be adjusted and this may also affect the results[19].

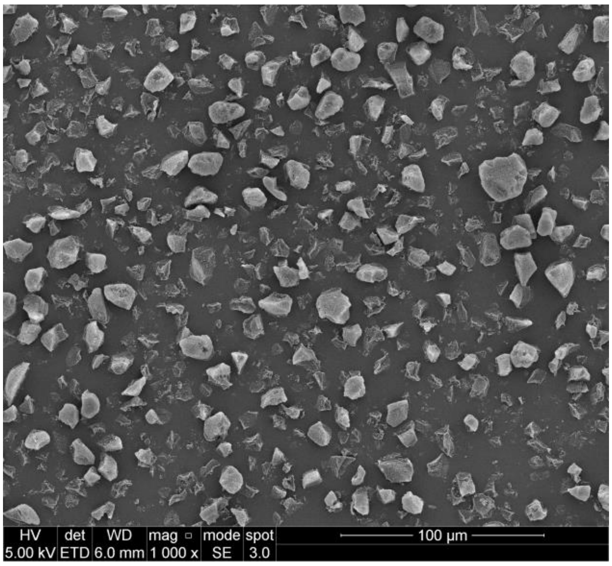

a) Type 1 – SEM image at 100 μm

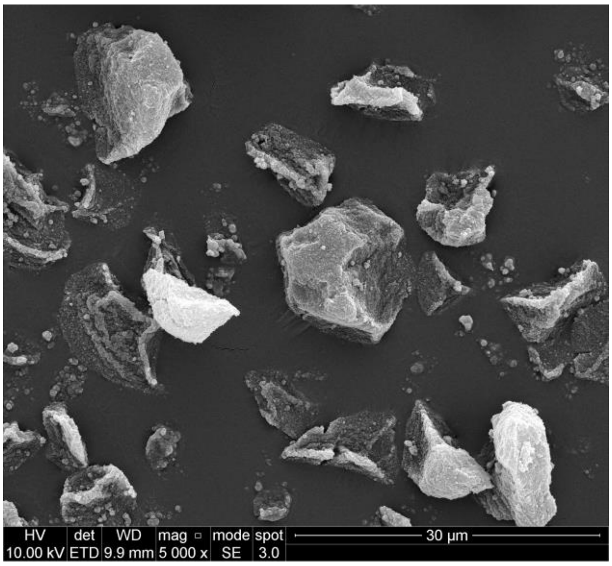

b) Type 1 – SEM image at 30 μm

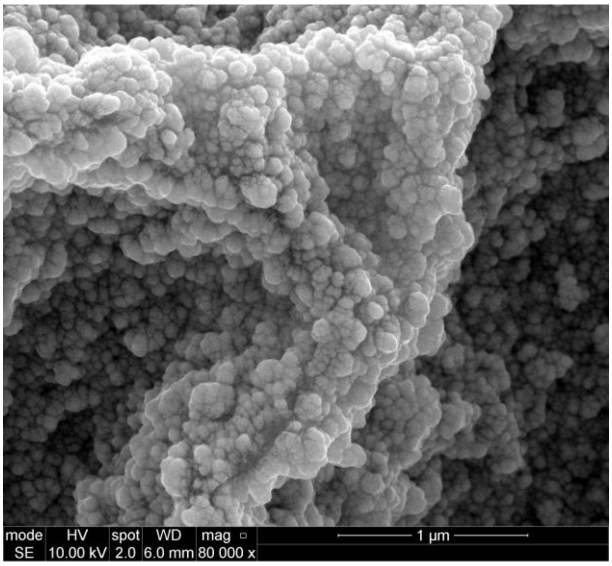

c) Type 1 – SEM image at 1 μm

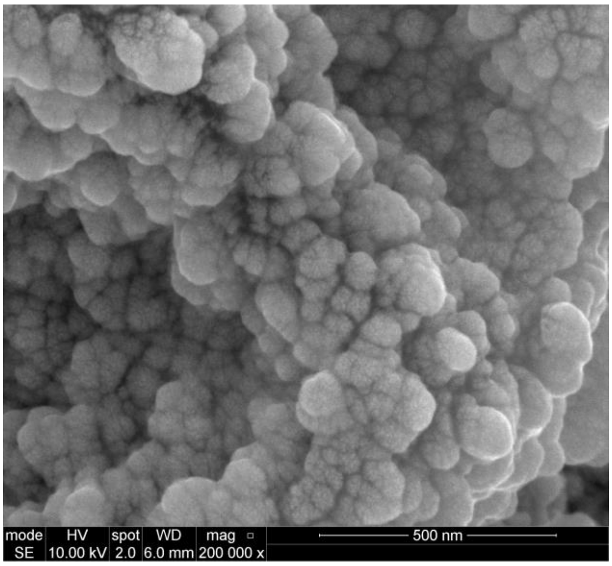

d) Type 1 – SEM image at 500 nm

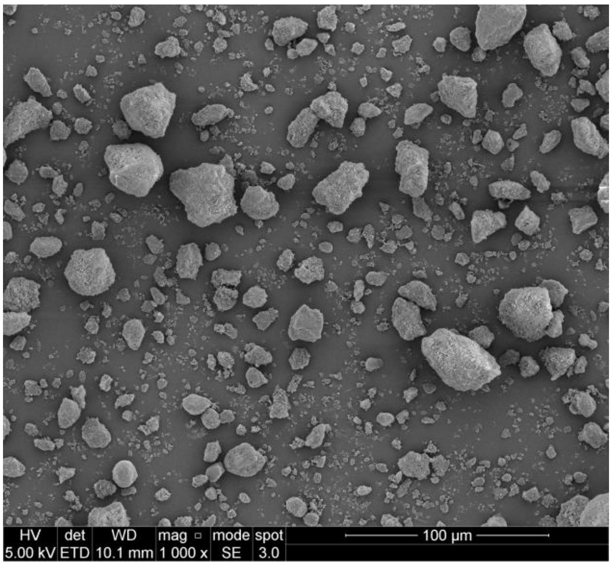

e) Type 2 – SEM image at 100 μm

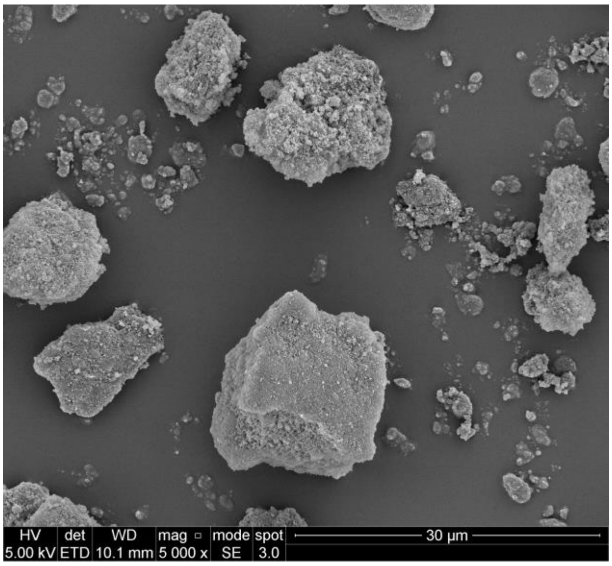

f) Type 2 – SEM image at 30 μm

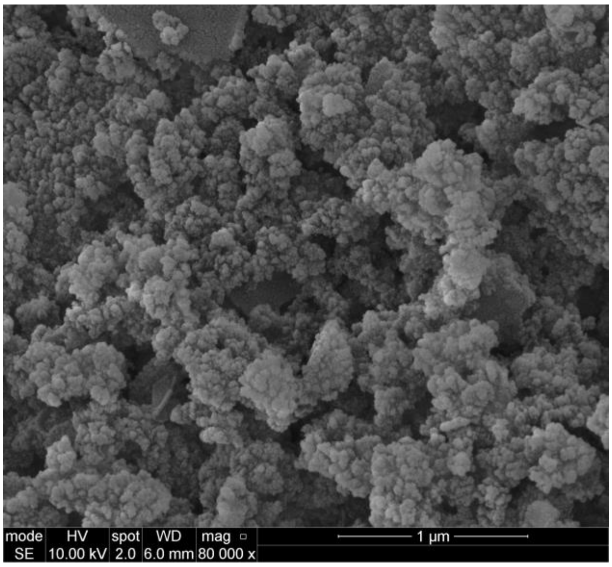

g) Type 2 – SEM image at 1 μm

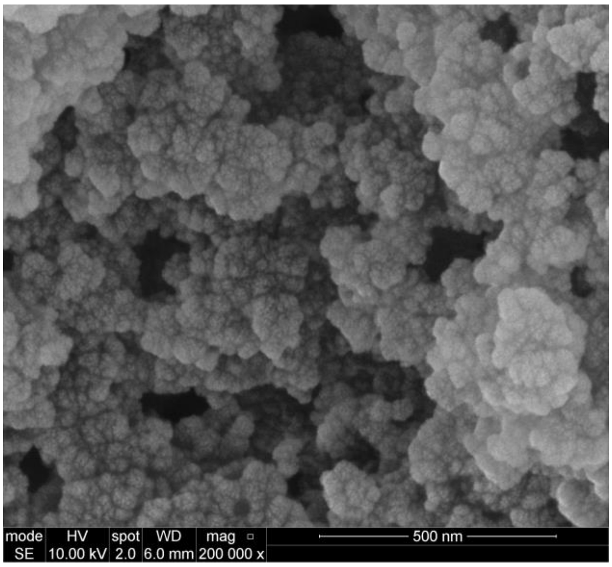

h) Type 2 – SEM image at 500 nm

Figure 1. SEM images of Type 1 and 2 aerogels taken at different magnifications (1000 x (a) and (e), 5000 x (b) and (f), 80,000 x (c) and (g) and 200,000 (d) and (h)).

The skeletal material density was calculated from the mass and volume combined with the volume-pressure relationship of Boyle's law measured using the gas displacement method (Micrometrics AccuPyc 1330 Helium Pycnometer used at 20 °C). The result was 2430 kg/m^3 for Type 1 and 1710 kg/m^3 for Type 2. The bulk densities of these materials, ρ_b, were determined using calibrated scales: they were 38.71 kg/m^3 and 104.91 kg/m^3 for aerogel particle Types 1 and 2, respectively.

a) Type 1 – Enova IC3100 b) Type 2 – JIOS AeroVa D20

Figure 2. Photographs of the powder samples used in the impedance tube experiments.

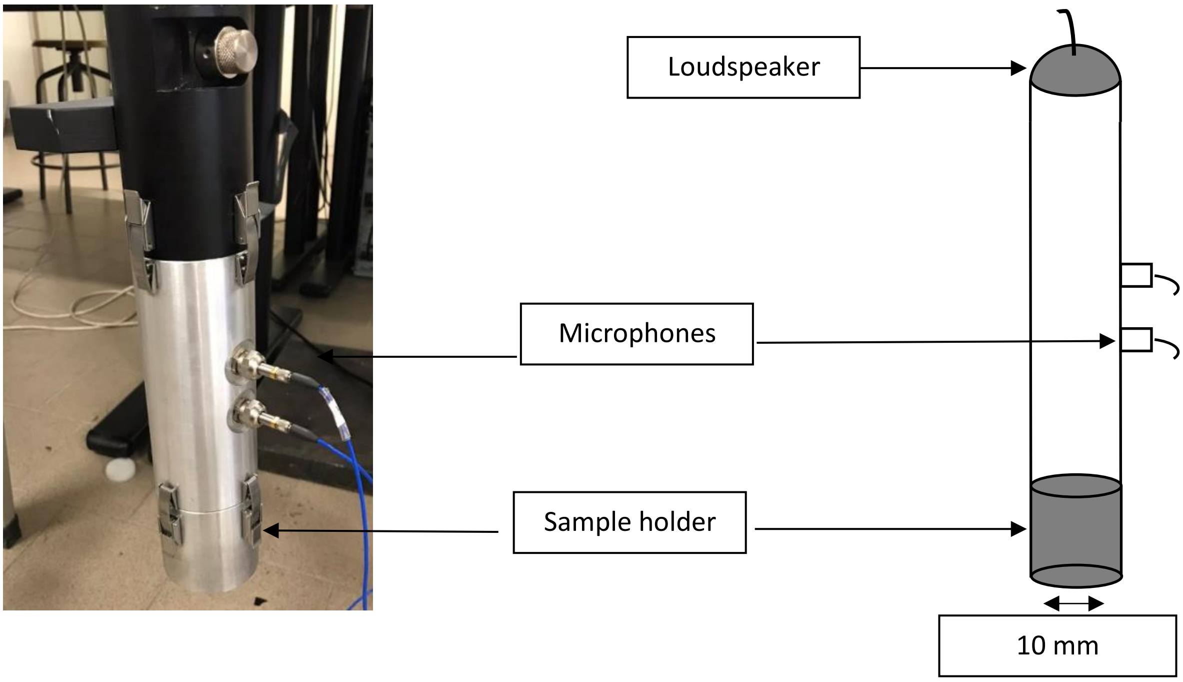

Figure 3. 2-microphone impedance tube setup to measure the surface impedance of a porous layer (taken with permission from ref. 26).

The acoustical properties of the aerogel stacks were measured in a 10 mm diameter standing wave tube which was custom made by Materiacustica[27]. This 2-microphone tube setup was developed to test small material specimens such as granular media and powders in accordance with the ISO standard 10534-2:2001[23]. This setup enabled measurement of the normalized surface acoustic impedance, complex reflection coefficient and sound absorption coefficient of a hard-backed porous layer in the frequency range from 100 to 4999 Hz. The spacing between the two microphones was 30 mm, which is usual for this frequency range as recommended in the ISO standard[23]. The distance from the sample surface to the first microphone was 85.9 mm. The thickness of all the samples used in the acoustic experiments was 50 mm. Figure 2 shows the Type 1 and Type 2 aerogel powders which were used in the acoustic experiments. Finally, Figure 3 shows a photograph and sketch of the vertically standing wave tube that was used in these experiments. Note that all sound pressure levels quoted here refer to the sound wave incident on the sample, integrated over the frequency range 100 to 4999 Hz.

III. Modelling of aerogel granule stacks

It was observed from the experimental data that the acoustical absorption coefficients of the tested aerogel granule stacks differed significantly from those that would be expected from a conventional sound absorber such as a layer of polymeric fibers. The acoustic absorption coefficient of the aerogel layers showed multiple, lightly damped depth resonances: an example, the normal incidence sound absorption coefficient measured at different incident, broadband sound pressure levels [dB] for the two types of materials are shown in Figure 4. Notably, large peak values of absorption appear at unusually low frequencies. It was also found that the heights of these peaks decreased with increasing sound pressure level, which provides the main evidence that the aerogel sample stacked in the tube behaves non-linearly. It was also clear when conducting the experiments that the granules comprising the powder samples vibrated under acoustic excitation. That vibration caused some dispersion of powder particles over the area of the impedance tube adjacent to the sample holder. The sample thickness occasionally reduced by as much as 0.5 mm after the first time the acoustic stimulus was applied. There was little or no subsequent change in the sample thickness when the experiment was repeated without touching the sample. At this stage the experimental data were recorded and used for the comparison with the model.

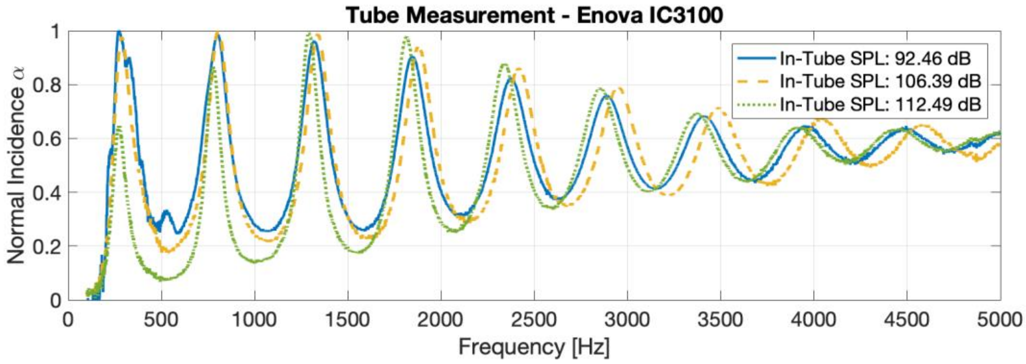

a)

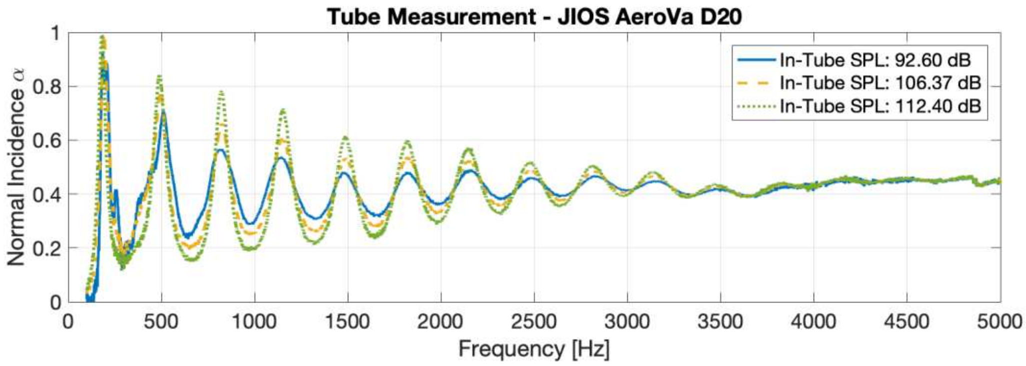

b)

Figure 4. Normal incidence sound absorption coefficients, *α*'s, measured at different in-tube sound pressure levels in standing wave tube experiments for (a) Enova IC3100 and (b) JIOS AeroVa D20. The SPL shown in the legend corresponds to the incident, broadband sound pressure levels measured with the two microphones in accordance with 23.

A. Acoustical Theories for Predicting Sound Absorption

In the present work two models were used to predict the frequency-dependent equivalent density, ρ_e, and bulk modulus, K_f, of the fluid phase (i.e., air) in the aerogel granule stacks: (i) the 5-parameter Johnson-Champoux-Allard (JCA) model[28,29]; and (ii) the 3-parameter Páde approximation (3P) model[30]. The Biot theory[31] (also see Chapter 11 in ref. 2) was then applied to account for the frame elasticity in the presence of air.

B. Bulk modulus and equivalent density predictions with the JCA model

The original JCA model requires five non-acoustic parameters as inputs: (i) airflow resistivity, σ; (ii) porosity, ϕ; (iii) tortuosity, α_∞; (iv) viscous characteristic length, Λ; and (v) thermal characteristic length, Λ'. Note that the static thermal permeability, k'_0[32] (denoted as q'_0 on pages 84–85 in ref. 2), is also considered as a thermal-effects contributor to the bulk modulus in the extended JCA-Lafarge (JCAL) model, but it was not used as an input to the JCA model that was applied in the current study. Also, note that for fibrous media as described in Ref. 5, Λ and Λ' were calculated as functions of σ, ϕ, α_∞[30] and the shape factors, c (usually equaling 1 for fibers) and c' (i.e., $c'=\Lambda/\Lambda'$). In contrast, σ, ϕ, α_∞, Λ and Λ' were used in the current study to calculate ρ_e and K_f based on the JCA model (eqs. (3) and (18) in ref. 28). Other ambient parameters needed for the modeling process included the dynamic viscosity of air, η=1.82×10^{-5} Pa s, the speed of sound in air, c_0=343 m/s, the density of air, ρ_0=1.21 kg/m^3, the Prandtl number, B^2=0.71, and the specific heat ratio, γ=1.402.

C. Bulk modulus and equivalent density predictions with the 3-parameter model

The 3-parameter (3P) model described in 30 was also adopted as a simpler alternative to the JCA model to predict the aerogel's bulk modulus and effective density. These properties were then used in the Biot model[31] to account for the response of the poro-elastic nature of the aerogel stacks. The 3P model makes use of the median pore size, s_b, porosity, ϕ, and standard deviation of the pore size, σ_s. It is assumed that the median pore size, standard deviation in pore size, two characteristic lengths, flow resistivity and tortuosity are inter-related[30]: i.e.,

$$\Lambda = \bar{s}e^{-5/2(\sigma_s \log 2)^2} \tag{1}$$

$$\Lambda' = \bar{s}e^{3/2(\sigma_s \log 2)^2} \tag{2}$$

$$\alpha_\infty = e^{4(\sigma_s \log 2)^2} \tag{3}$$

$$\sigma = \frac{8\eta\alpha_\infty}{\bar{s}^2\phi}e^{6(\sigma_s \log 2)^2}. \tag{4}$$

The parameters defined by eqs. (1)-(4) were then used as inputs to calculate the effective density, ρ_c, and bulk modulus, K_p, of the equivalent fluid representation[28,29] of the aerogel granule stack. Alternative equations for calculating these two properties can be found in the original paper by Horoshenkov et al. (ref. 30, eqs. (13) and (16)).

D. Effective density and bulk modulus as inputs in the Biot poro-elastic model

The JCA model outputs, ρ_e and K_f, could be used together with the aerogel's σ, ϕ, α_∞, its bulk density, ρ_b, and/or its elasticity parameters (Young's modulus, E_1, Poisson's ratio, v, and mechanical loss factor, η_m) as bulk property inputs for the Biot poro-elastic theory (originally introduced in ref. 31, and whose formulations are summarized in Section 2.3 of ref. [5]). On the other hand, when the 3P model was applied, its outputs, ρ_c and K_p, were translated into effective density, ρ_e, and bulk modulus, K_f, of the fluid phase of the poro-elastic material to make them configurable as inputs for the subsequent calculations involving the Biot poro-elastic theory: i.e.,

$$\rho_e = \phi \rho_c^*, \tag{5}$$

$$K_f = \phi K_p^*, \tag{6}$$

where * denotes the complex conjugate, which is required owing to the difference in the adopted $e^{\pm i\omega t}$ convention in the two models (see refs. 29 and 30).

It should be noted that here the Biot poro-elastic theory was preferred instead of the Biot limp porous theory (also summarized in Section 2.3 of ref. 5) which makes it possible to introduce a small, but finite value of E_1 for the aerogel stack's elastic frame. In that case, a frequency-dependent η_m can be used to quantify the non-linearity of the material's loss mechanism in the low frequency regime shown in the experimental data. Finally, the layer depth, d, was used as a bulk property to calculate the sound absorption of a finite depth layer by using either the transfer matrix method (TMM)[33] or the arbitrary coefficient method (ACM)[34], both of which functioned equivalently.

IV. Results & Discussion – Characterization of Acoustical-Related Bulk Properties

A. Fitting the measured sound absorption coefficient spectra

The characterization of the bulk properties was carried out by fitting the two models described in Section III to the measured frequency-dependent absorption coefficients for the Type 1 and Type 2 aerogels. This fitting process was based on the MATLAB built-in numerical optimization function “particleswarm”. Occasionally, a manual and empirical adjustment of the parameter inputs was required. To be more specific, by fixing η_m=0.2, E_1=775 Pa and v=0.396, the parameters σ, ϕ, α_∞, Λ, Λ', ρ_b, were fitted as constant values by using the JCA-Biot-poro-elastic-TMM/ACM model, and s_b, ϕ, σ_s, ρ_b were fitted as constant values by using the 3P-Biot-poro-elastic-TMM/ACM model for Type 1 aerogel granule stacks. Then, all the fitted bulk properties mentioned above, except for ρ_b, were used to fit the data for Type 2 aerogel granule stacks. These parameters were not dominant, i.e., most significant, in the fitting process. Finally, η_m was manually adjusted from constant to frequency-dependent at each in-tube sound pressure level for both types of aerogels, with all the other bulk properties fixed to previously fitted values. Note that the loss factor *was* a dominant parameter. Also note that the detailed process of the development of frequency-dependent (“dynamic”) loss factor groups is described in a later part of this section. We note that both E_1 and v were estimated values in order to represent a finite, but small, elasticity of the aerogel stack’s solid frame.

Tables 1 and 2 present the summary of the input parameters identified inversely by using the JCA and 3P models, respectively. The measured and predicted normal incidence absorption coefficients for Type 1 and Type 2 aerogel powders are shown in Figures 5(a) and 6(a), respectively. These figures present the results for the range of incident sound pressure levels used in these tests. Recall that the broadband sound pressure level was calculated by combining the narrow band sound pressure levels measured at the frequency points from 100 to 4999 Hz for which the absorption coefficient data was provided. This information was available as a standard report generated for each measurement taken with the Materiacustica impedance tube. The narrow band sound pressure levels were calculated using the Fourier spectrum for the sound pressure with the 2-microphone procedure detailed in Refs. 23,26. By comparing the JCA-based (orange) and 3P-based (green) simulations of the sound absorption spectra, it can be seen that both models can very accurately predict the sound absorption performance for the target aerogel materials, especially in the low and medium frequency range below 2000 Hz. To further evaluate the prediction accuracy, the spectra of cumulative squared error from 100 Hz to 4999 Hz, between model-predicted and experiment-measured sound absorption are plotted in Figures 5(b)-(c) and 6(b)-(c) for the Type 1 and Type 2 materials, respectively, with the total root mean squared errors marked in the legends. It can be seen from the latter results that the two models represent the experimental result with very similar accuracy.

Table 1. Bulk properties characterized by fitting the JCA-Biot-TMM/ACM[29,33,34] with the measurements and used to predict sound absorption coefficient spectra.

Material	σ [Rayls/m MKS]	ϕ	α_∞	Λ [μm]	Λ' [μm]	ρ_b [kg/m^3]	E_1 [Pa]	v	η_m
Type 1	10.5×10^6	0.999	3.0	36.1	36.1	35.5	775	0.396	Eq. (7) and Table 3
Type 2	10.5×10^6	0.999	3.0	36.1	36.1	94.0	775	0.396	Eq. (7) and Table 3

Table 2. Bulk properties used for the 3P-Biot-TMM/ACM[30,33,34] to predict sound absorption coefficient spectra.

Material	ϕ	s_b [μm]	σ_s	ρ_b [kg/m^3]	E_1 [Pa]	v	η_m
Type 1	0.999	14.7	0.756	35.5	775	0.396	Eq. (7) and Table 3
Type 2	0.999	14.7	0.756	94.0	775	0.396	Eq. (7) and Table 3

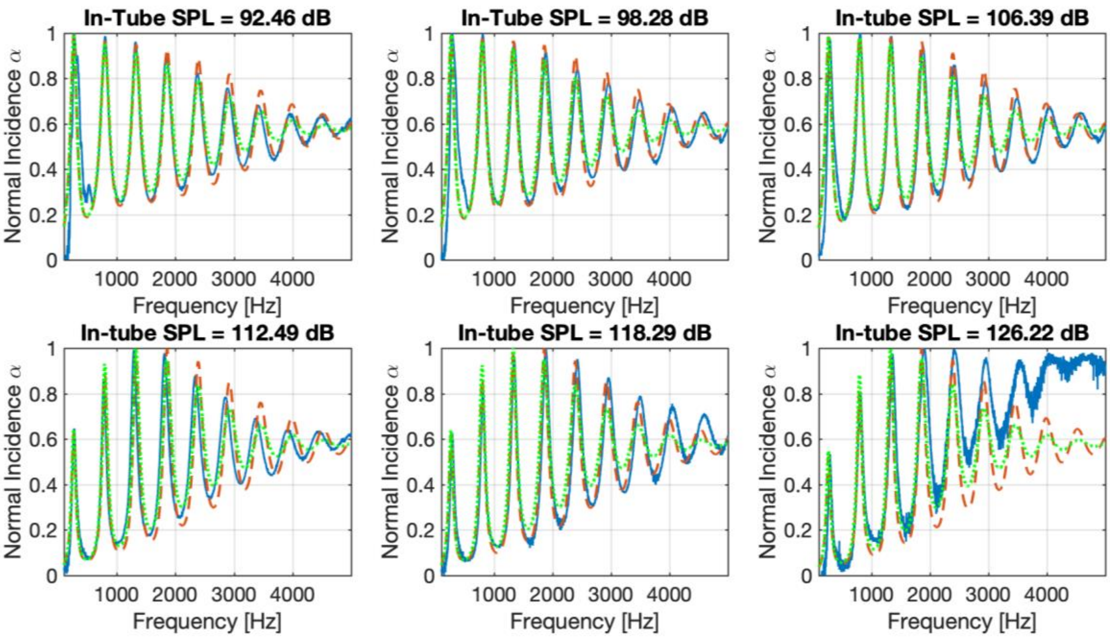

a)

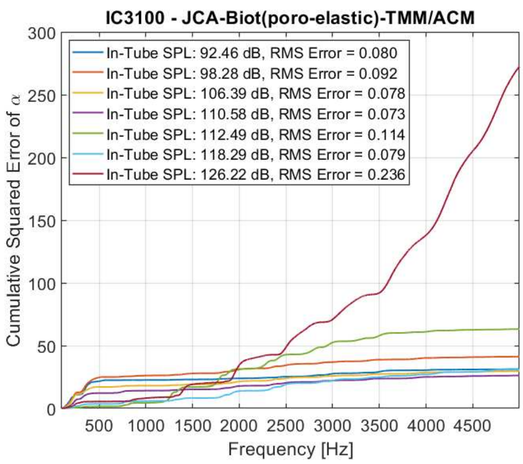

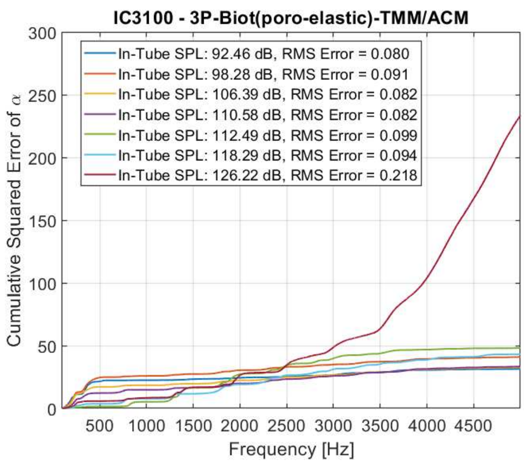

b) c)

Figure 5. (a) Normal incidence absorption coefficients, α's, of Enova IC3100 (Type 1) at different incident sound pressure levels by experimental measurement (blue-solid lines), the JCA-Biot(poro-elastic)-TMM/ACM model prediction (orange-dashed lines), the 3P-Biot(poro-elastic)-TMM/ACM model prediction (green-dotted lines), (b) Cumulative squared error between JCA-Biot(poro-elastic)-TMM/ACM model prediction and experimental measurement,

and (c) Cumulative squared error between 3P-Biot(poro-elastic)-TMM/ACM model prediction and experimental measurement.

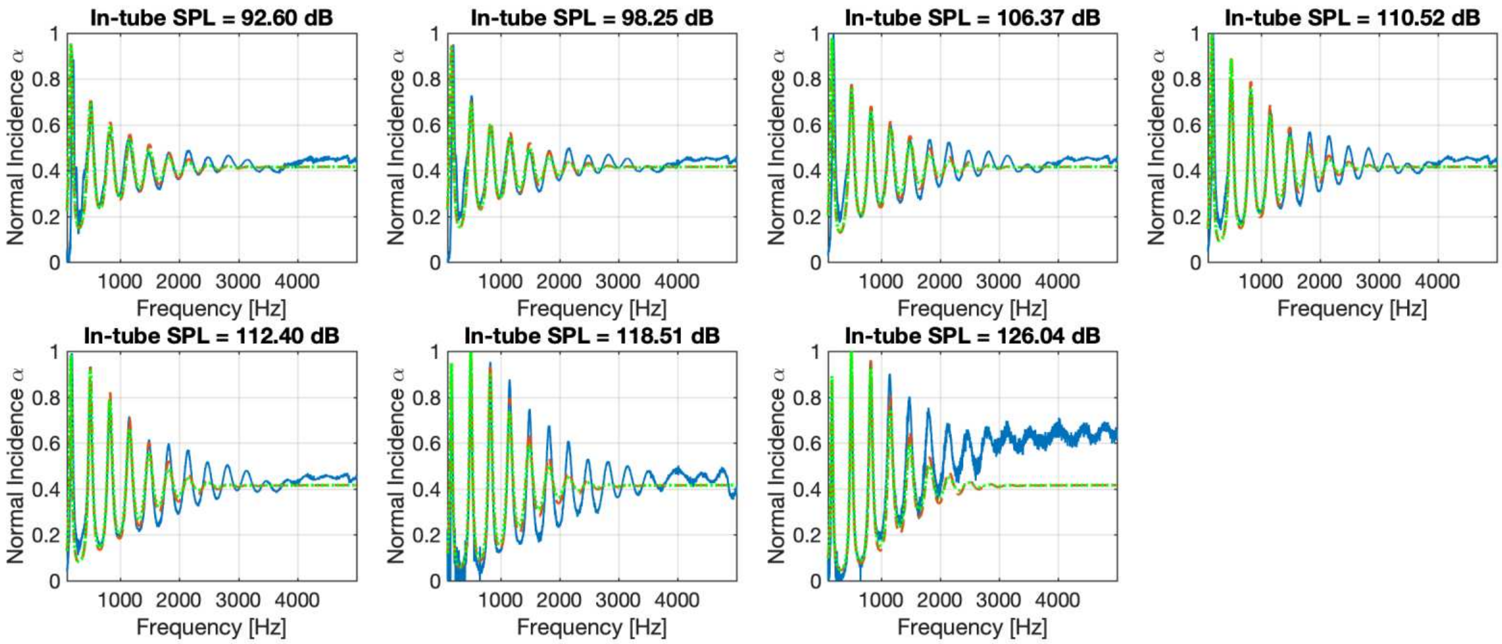

a)

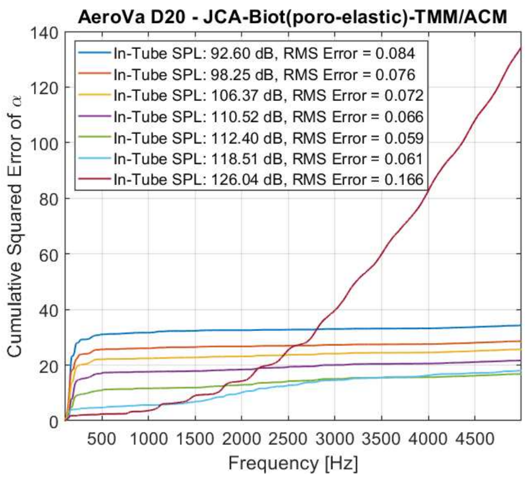

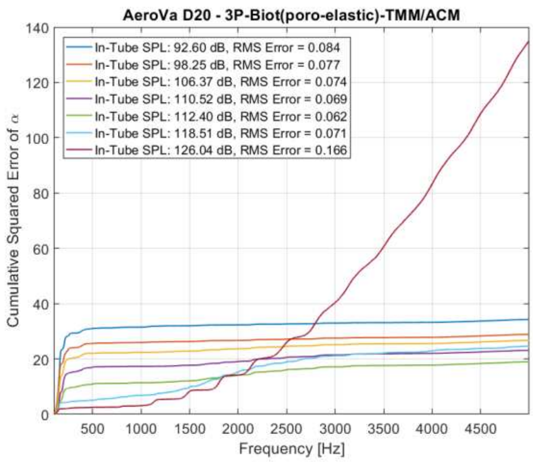

b) c)

Figure 6. Normal incidence absorption coefficients, α's, of JIOS AeroVa D20 (Type 2) at different incident sound pressure levels by experimental measurement (blue-solid lines), the JCA-Biot(poro-elastic)-TMM/ACM model prediction (orange-dashed lines) and the 3P-

Biot(poro-elastic)--TMM/ACM model prediction (green-dotted lines), (b) Cumulative squared error between JCA-Biot(poro-elastic)-TMM/ACM model prediction and experimental measurement, and (c) Cumulative squared error between 3P-Biot(poro-elastic)-TMM/ACM model prediction and experimental measurement.

The predicted sound absorption coefficient spectra were calculated at the 4900 equally spaced frequencies ranging from 100 to 4999 Hz in the fitting process to match the frequency step in the measured data. This congruence allowed the introduction of a 4900-step loss factor that decreased logarithmically with increasing frequency, f: i.e.,

$$\log_{10}\eta_m = af + b. \quad (7)$$

That formal dependence primarily was the factor that enabled good fitting of the model to the measured absorption coefficient spectra, especially at low frequencies for both materials, and it allowed the non-linearity of both materials' acoustical performance to be numerically captured. Particularly, it was found that the coefficients a and b in eq. (7) depend on the incident sound pressure falling on the sample: their values are given in Table 3. The dependence of these coefficients on the sound pressure level is also plotted in Figures 7 and 8 for Type 1 and Type 2 aerogels, respectively. These coefficients have a clear physical meaning. The absolute value of coefficient a is the rate with which the loss factor decreases with increasing frequency, i.e., the greater it is, the less this loss factor would depend on the frequency. The value of the coefficient b is the low-frequency limit of the loss factor, i.e., the greater it is, the greater the losses associated with the frame vibration excited by the incident sound wave when the frequency of sound is relatively low.

The behavior of these two coefficients is illustrated graphically in Figures 7 and 8. These data suggest that the dependence of the loss factor on the frequency for the relatively low bulk density Type 1 aerogel is not strongly affected by the sound pressure level (see Figure 7). In the case of Type 2 aerogel, however, there is a rapid increase in the absolute value of a when the sound pressure level reaches 110 dB. This means that the dependence of the loss factor on the frequency becomes much more pronounced, i.e., the losses associated with mechanical vibration of a denser aerogel reduce much more rapidly as the frequency increases.

The behavior of the coefficient b on the sound pressure level is rather similar for the two aerogels as illustrated in Figure 8. Below 105 dB the value of this coefficient does not depend very significantly on the type of aerogel or the sound pressure level. Above this threshold however, the value of b drops suddenly and then continues to reduce slowly with increasing sound pressure level. This behavior suggests that there is sudden drop in the loss factor near the level of 105 dB. The absolute value of this drop was considerably greater in the case of the lighter aerogel (Type 1) suggesting that the drop in the losses caused by a more intense incident sound wave is greater when the bulk material density is lighter.

Table 3. The coefficients in the equation for the dynamic loss factor (eq. (7)) for two aerogels.

Type 1			Type 2		
In-tube SPL [dB]	a	b	In-tube SPL [dB]	a	b
92.46	-5.511×10^{-4}	1.353	92.60	-5.307×10^{-4}	1.333
98.28	-5.520×10^{-4}	1.335	98.25	-5.720×10^{-4}	1.358
106.39	-6.328×10^{-4}	1.318	106.37	-6.328×10^{-4}	1.277
110.58	-6.328×10^{-4}	1.141	110.52	-6.736×10^{-4}	1.071
112.49	-6.328×10^{-4}	0.761	112.40	-7.144×10^{-4}	1.017
118.29	-6.736×10^{-4}	0.768	118.51	-1.470×10^{-3}	1.046
126.22	-6.940×10^{-4}	0.649	126.04	-1.674×10^{-3}	0.969

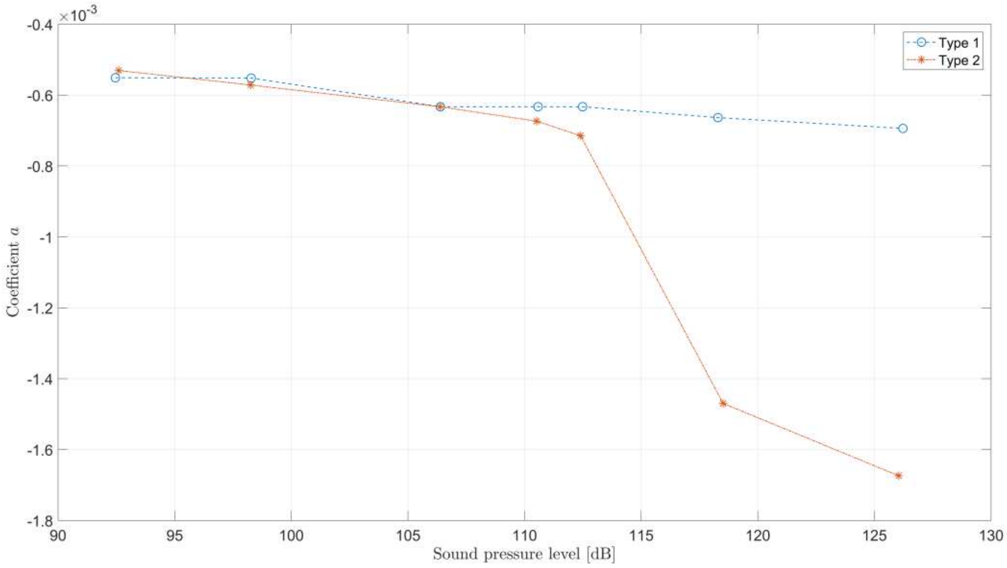

Figure 7. The dependence of the coefficient a in eq. (7) on the sound pressure level.

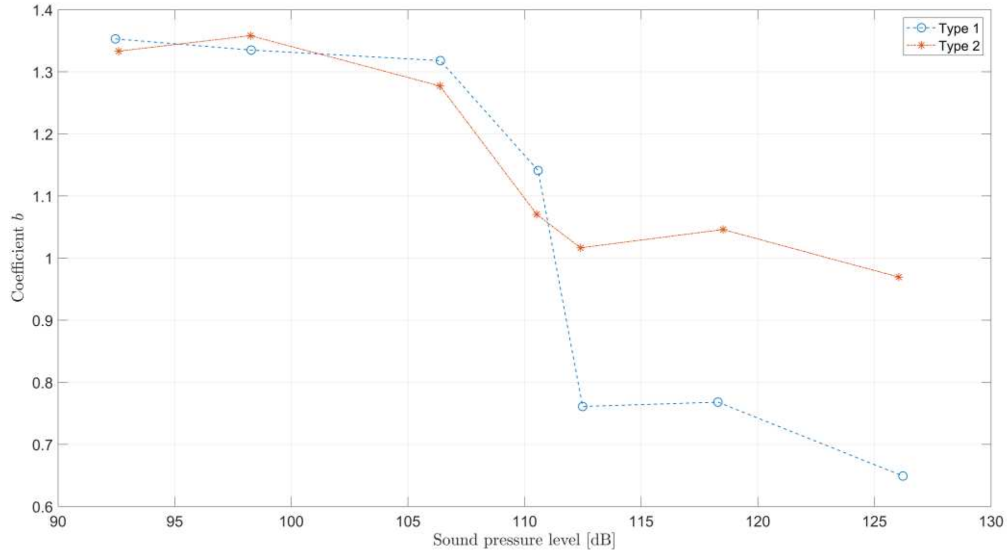

Figure 8. The dependence of the coefficient b in eq. (7) on the sound pressure level.

In light of these results, it may be of interest to estimate the radiation pressure acting on the aerogel particles. In the presence of an oscillatory flow, e.g., an incident sound wave, the drag force acting on an isolated aerogel particle with radius R is in Ref. 35

$$F = 6\pi\mu R\left(1+\frac{R}{\delta}\right)u + 3\pi R^2\sqrt{\frac{2\mu\rho_0}{\omega}}\left(1+\frac{2R}{9\delta}\right)\frac{\partial u}{\partial t} \quad (8)$$

where $\delta = \eta/(\rho_0\omega)$ is the viscous layer depth, ω is the angular frequency and u is the acoustic velocity in the incident sound wave. In the case of harmonic excitation, $u = u_0 \sin(\omega t)$ so that the derivative in eq. (8) is $\frac{\partial u}{\partial t} = \omega u_0 \cos \omega t$. Figure 9 shows the frequency-dependent, normalized drag force amplitude, $|F|$, acting on a particle with $2R$ = 14 μm diameter at the broadband sound pressure level of 112 dB. This diameter is similar to the mean particle diameter measured from the SEM images for the Type 1 and Type 2 aerogels studied in this work. The drag force predicted by eq. (8) was normalized against the particle gravity force, $F_g = 4/3R^3\rho_b g$, where g is the gravity acceleration. The acoustic velocity amplitude, u_0, in eq. (8) was estimated by using the narrow band incident sound pressure levels measured at the sample surface and surface impedance of the sample. The data shown in Figure 9 suggest that for Type 1 aerogel the drag force almost always exceeds the gravity force at this level of excitation, i.e., the aerogel particles are likely to vibrate at a range of frequencies, particularly at resonance frequencies. These resonance frequencies in $|F/F_g|$ spectra coincide with the maxima in the absorption coefficient spectra shown in Figure 5. In the case of Type 2 aerogel, the normalized drag force is close to 1 near the resonance peaks which occur below 1000 Hz. Further increase in the sound pressure level will make this force exceed 1, which means that the particles of this aerogel will begin to vibrate under acoustic excitation.

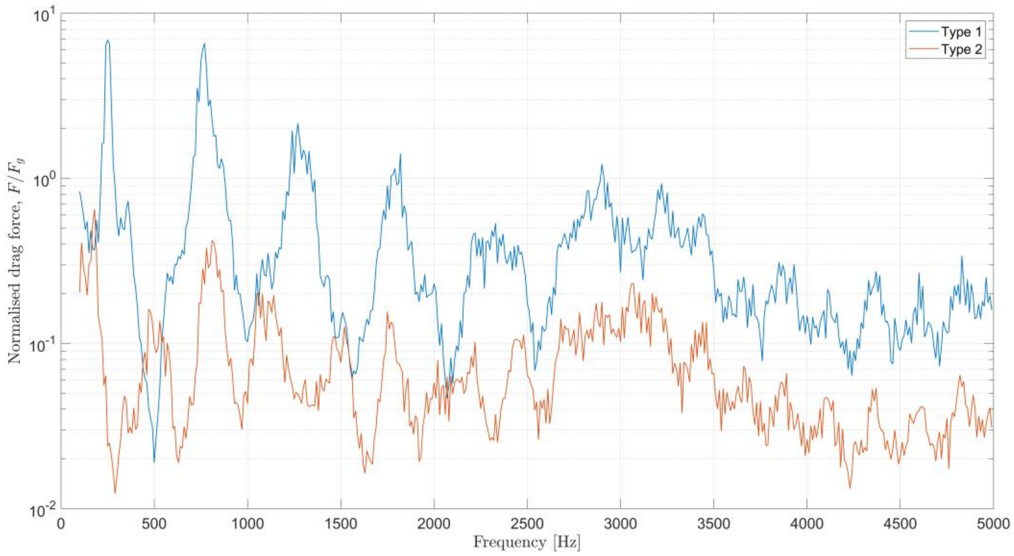

Figure 9. The spectra for the normalized drag force acting on a particle of Type 1 and Type 2 aerogel in the case of 112 dB broadband sound pressure level incident on the surface of the aerogel specimen in the impedance tube.

Figure 10 shows the estimates of the displacement spectra for the air molecules in the incident sound wave at 112 dB. This figure, and Figure 9, can explain the change in the absorption coefficient spectra with the increased sound pressure level. When the sound pressure level is relatively small, e.g., 92 dB (broadband), then the displacement in the incident sound wave is well below that of the particle diameter. The relatively light particles in Type 1 aerogel can begin to be excited by the vibrating air, particularly in the lower frequency range. However, their movements are likely to be much smaller than their diameter. In this way they interact mechanically with each other losing energy through contact friction so that the acoustic absorption coefficient peaks close to 1 at frequencies below 1000 Hz (see Figure 5 for 92 dB). As the level of excitation increases, the amplitude of the particle movement increases progressively. This amplitude generally reduces with the increased frequency. When this amplitude becomes comparable with the particle diameter, e.g., 1 μm at 250 Hz for 112 dB excitation (see Figure 10), the particles can begin to separate, i.e., they lose contact with each other, so that the losses reduce below 1000 Hz as illustrated by the standing wave tube data in Figure 5. At this level, the amplitude of the displacement of air molecules in the medium and high frequency regime (1000 – 3000 Hz) is close to the 1-10 nm range (around 1/1000th of the particle diameter) which seems ideal to result in an increase in the absorption coefficients, particularly around the resonance peaks as shown in Figure 5.

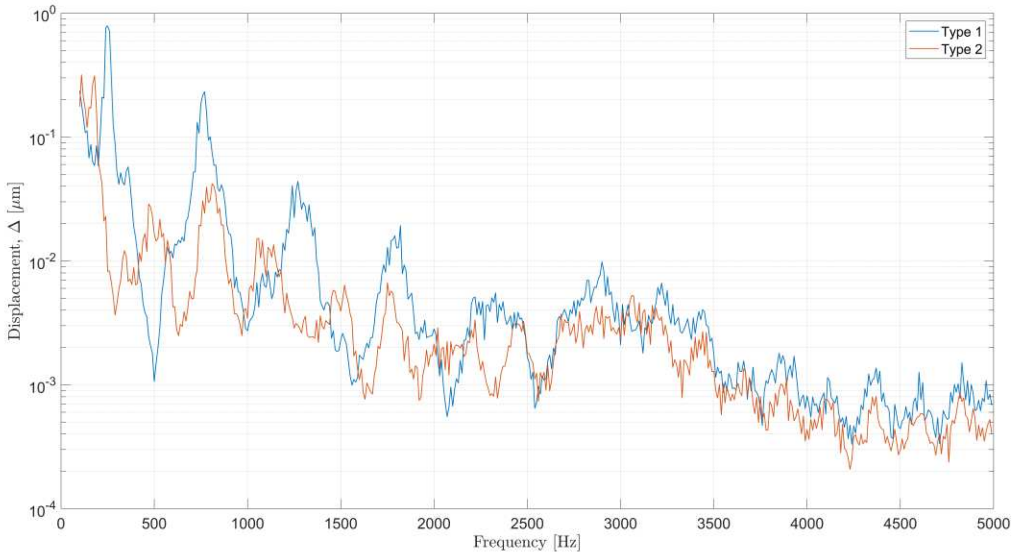

Figure 10. The spectra for the displacement of the air molecules in the sound wave incident on the surface of Type 1 and Type 2 aerogel specimen in the impedance tube.

Similar behavior can be seen in the case of the Type 2 aerogel (see Figure 6). However, this is a much denser material, so this behavior is much less pronounced because this denser material would require a much greater drag force to make its particles vibrate as shown in Figure 9. Nevertheless, it appears from the data that the amplitude, of the peaks in the absorption coefficient in the frequency range of 1000 to 2000 Hz almost double as the broadband sound pressure level increases from 92 to 126 dB (see Figure 6).

Furthermore, to prove that the dynamic loss factor groups in the Biot-poro-elastic theory are required to provide good fittings/predictions of target aerogel granule stacks' sound absorption performance especially at the low frequency region, both Biot-limp-porous theory and Biot-poro-elastic theory with constant loss factor (i.e. independent of frequency or in-tube sound pressure level) were used to predict the normal incidence sound absorption coefficients, and the predicted results are shown as comparisons with measured results in Appendix A. Neither of these models can predict the absorption coefficients as accurately as the poro-elastic model with frequency-dependent loss factor.

V. Conclusions

In the present work the acoustic absorption offered by two powder-form aerogels with particle sizes in the range of 5.54-41.78 μm was studied. Two theoretical models were fitted to the measured data. The 5-parameter Johnson-Champoux-Allard[28,29] and an alternative 3-parameter[30] models have been used in combination with the Biot poro-elastic model[31] to predict the acoustical properties of the aerogel layers and therefore to explain the measured data. A summary of main conclusions is as follows:

(1) A relatively thin (e.g., 50 mm thick) layer of a light aerogel powder can provide a very high (almost 100%) acoustic absorption at relatively low frequencies, e.g., below 250 Hz.

(2) The behavior of these materials is non-linear, i.e., it depends on the amplitude of the incident sound pressure.

(3) The agreement between the predicted and measured absorption coefficient obtained with the adopted models was close with, root mean squared errors below 0.1, for most of the in-tube sound pressure levels and with the given quoted set of the input parameters.

(4) Reasonable bulk densities were captured by the numerical fitting function, which showed that the Type 2 (94 kg/m^3) aerogel had a density more than twice that of Type 1 (35.5 kg/m^3), but both bulk densities characterized by the models were smaller than the values directly measured using material samples (Type 1: 38.7 kg/m^3, Type 2: 104.9 kg/m^3) This indicated that the aerogel's mass density might vary under different in-tube sound pressure levels and loading conditions (i.e. standing wave tube input voltages) due to non-linearity.

(5) A small but finite elasticity expressed in terms of the Young's modulus of both materials' solid frame structure needs to be introduced in the modeling process in order to realize a good fitting to the measured sound absorption over a broad range of frequencies.

(6) Different groups of dynamic loss factors were needed to yield “best fits” at different in-tube sound pressure levels, which indicates that the non-linearity of both materials quantified in terms of dynamic loss factor is dependent on both frequency and incident sound pressure level.

(7) An additional sound absorption mechanism could not be captured by the Biot-type poro-elastic model and needs to be considered to provide better fits in the high frequency region (i.e., above 2000 Hz) especially when the incident sound pressure level is relatively large.

(8) The loss factor required to fit the measured data at low frequencies (i.e., below 2000 Hz) is very high, and is higher than is physically reasonable for an elastic porous medium, which then suggests that there is an additional loss mechanism working at low frequencies to contribute to the non-linearity of the sound absorption.

Detailed investigation of aspects (6) to (8) in addition to a summary of design concepts for optimizing aerogel granule stacks’ wide-band sound absorption should be the subject of future work. These design concepts can be based on the calculations of the fluid displacement and resulting drag force acting on the aerogel particle that offer an explanation of the observed level-dependent acoustic absorption behavior of the aerogel stacks.

Acknowledgements

The authors would like to thank the EPSRC-sponsored Centre for Doctoral Training in Polymers, Soft Matter and Colloids (EP/L016281/1) at The University of Sheffield for their financial support of this work. We would also like to thank our industry partner Armacell and Dr Mark Swift and Mr. Pavel Holub for their continued support throughout this research study. We extend our thanks to Dr Ian Ross at the University of Sheffield, Sorby Centre, for taking high magnification SEM images.

Appendix A. Demonstration of the necessity to introduce dynamic loss factors in the Biot-poro-elastic theory

First, the Biot limp porous theory [2] was used to predict sound absorption coefficients given the properties listed in Table 1 (except for E_1, v, and η_m, and the same inputs for all tube voltages) by following the JCA-Biot (limp porous)-TMM/ACM calculation routine, and the results are plotted as magenta-dashed lines in Figures 11(a-c) and 12(a-c) for the Type 1 and Type 2 materials, respectively. Secondly, the Biot-type poro-elastic model with a constant η_m=0.2, was used to predict sound absorption coefficients given the properties listed in Table 1 (except for η_m, same inputs for all tube voltages) by following the JCA-Biot(poro-elastic)-TMM/ACM calculation routine, and the results are plotted as black-dotted lines in Figures 11(a-c) and 12(a-c) for Type 1 and Type 2 particles, respectively.

It can be observed that by using either Biot-limp-porous theory or Biot-poro-elastic theory with a constant loss factor, we could not realize predictions are accurate as were obtained previously with a frequency-dependent loss factor, especially in the frequency region below 2000 Hz. This demonstrated that it is necessary to introduce the dynamic loss factor as a function of frequency in the Biot-type poro-elastic theory to yield a robust prediction of sound absorption coefficients. That conclusion is reinforced by examining the cumulative error plots also presented in Figures 11(a-c) and 12(a-c). It can be seen that the errors are very much larger for these models than was the case for the results plotted in Figures 5 and 6.

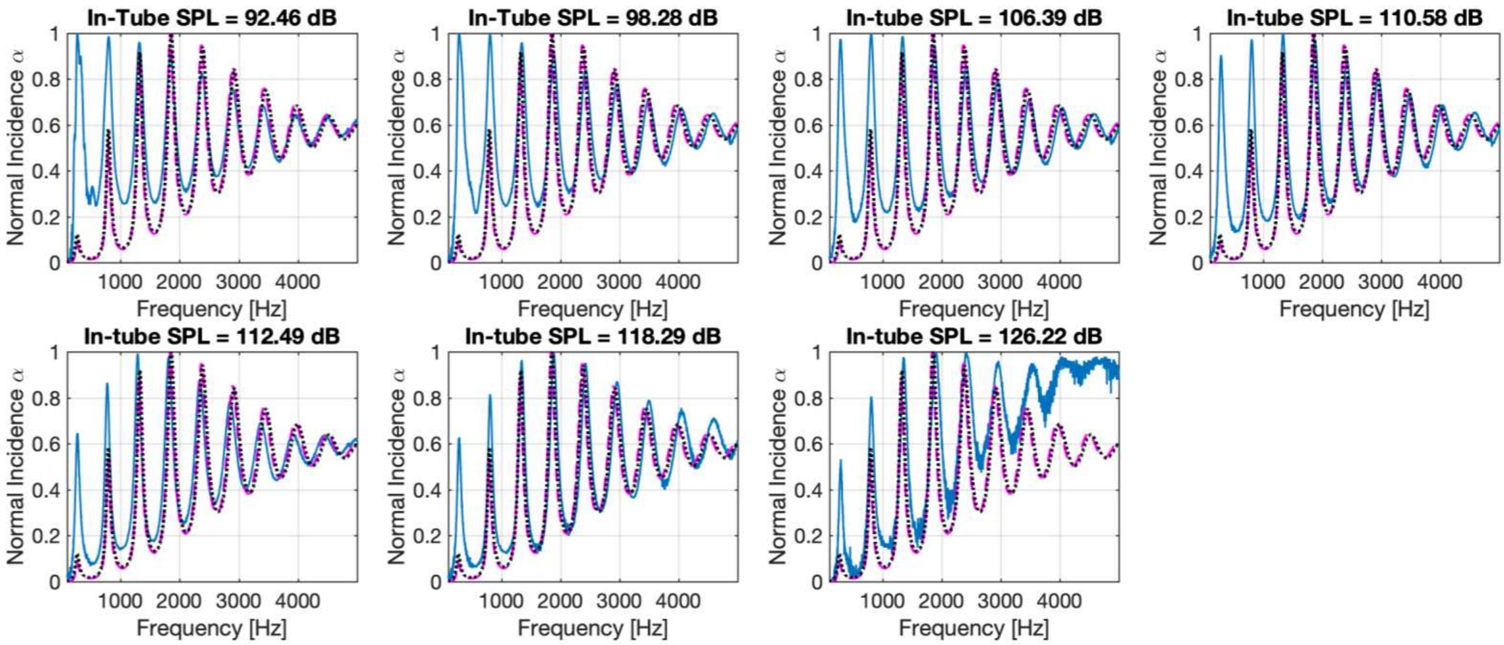

a)

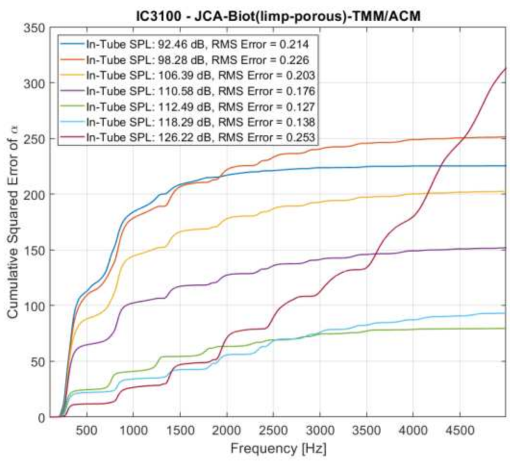

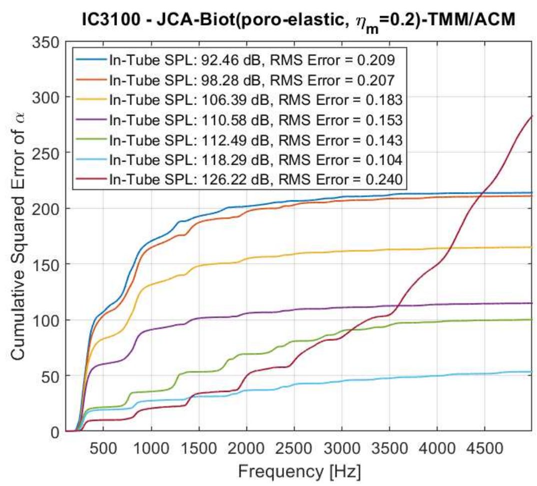

b) c)

Figure 11. (a) Normal incidence absorption coefficients, α's, of Enova IC3100 (Type 1) at different incident sound pressure levels (i.e., tube voltages) by experimental measurement (blue-solid lines), the JCA-Biot(limp porous)-TMM/ACM model prediction (magenta-dashed lines), the JCA-Biot(poro-elastic)-TMM/ACM model prediction (black-dotted lines) with constant η_m=0.2, (b) Cumulative squared error between JCA-Biot(limp-porous)-TMM/ACM model prediction and experimental measurement, and (c) Cumulative squared error between

JCA-Biot(poro-elastic with constant η_m)-TMM/ACM model prediction and experimental measurement.

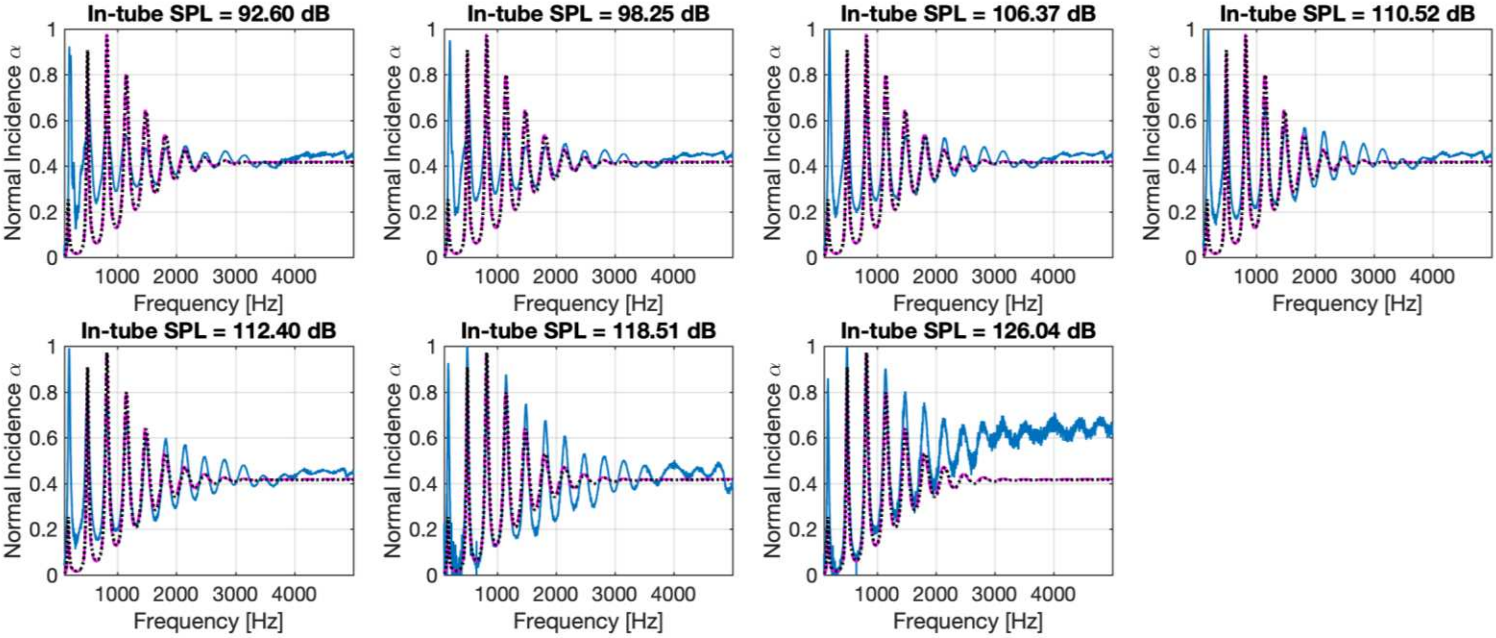

a)

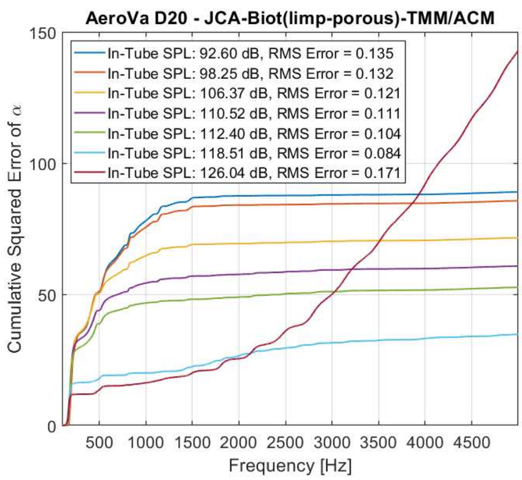

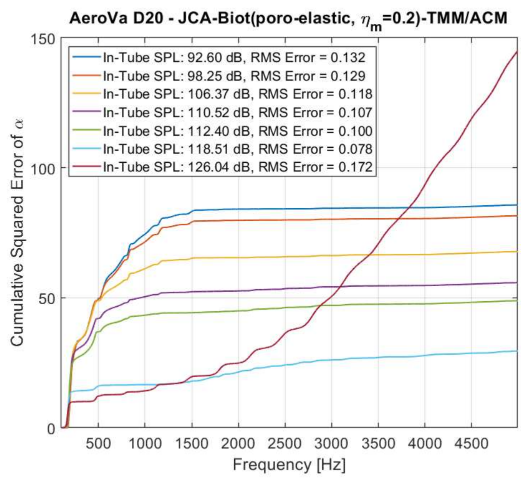

b) c)

Figure 12. (a) Normal incidence absorption coefficients, α's, of JIOS AeroVa D20 (Type 2) at different incident sound pressure levels (i.e., tube voltages) by experimental measurement (blue-solid lines), the JCA-Biot(limp porous)-TMM/ACM model prediction (magenta-dashed

lines), the JCA-Biot(poro-elastic)-TMM/ACM model prediction (black-dotted lines) with constant η_m=0.2, (b) Cumulative squared error between JCA-Biot(limp-porous)-TMM/ACM model prediction and experimental measurement, and (c) Cumulative squared error between JCA-Biot(poro-elastic with constant η_m)-TMM/ACM model prediction and experimental measurement.

References

[1]J. Yeo, Z. Liu, T.Y. Ng, "Silica Aerogels: A Review of Molecular Dynamics Modelling and Characterization of the Structural Thermal, and Mechanical Properties," In: Andreoni W., Yip S. (eds) Handbook of Materials Modeling. Springer, Cham. 1–22 (2018), https://doi.org/10.1007/978-3-319-50257-1_83-1.

[2]J.-F. Allard and N. Atalla, Propagation of Sound in Porous Media: Modeling Sound Absorbing Materials (2nd ed. Wiley, Chichester, 2009), pp. 327.

[3]Y. Xue, J.S. Bolton, "Microstructure design of lightweight fibrous material acting as a layered damper for a vibrating stiff panel," *J. Acoust. Soc. Am.* **143(6)**, 3254–3265 (2018), https://doi.org/10.1121/1.5038255.

[4]Y. Xue, J.S. Bolton, T. Herdtle, S. Lee, R.W. Gerdes, "Structural damping by lightweight poro-elastic media", *J. Sound Vib.* **459**, 114866 (2019), https://doi.org/10.1016/j.jsv.2019.114866.

[5]Y. Xue, "Modeling and design methodologies for sound absorbing porous materials when used as layered vibration dampers," PhD dissertation, Purdue University (2019).

[6]A. Khan, "Vibro-acoustic products from recycled raw materials using a cold raw extrusion process. A continuous cold extrusion process has been developed to tailor a porous structure from polymeric waste, so that the final material possesses vibro-acoustic properties," PhD thesis, Chapter 2, University of Bradford (2010).

[7]N.N. Voronina, K.V. Horoshenkov, "A new empirical model for the acoustic properties of loose granular media," *Appl. Acoust.* **64**, 415–432 (2003), https://doi.org/10.1016/S0003-682X(02)00105-6.

[8]R. Venegas, O. Umnova, "Acoustical properties of double porosity granular materials," *J. Acoust. Soc. Am.* **130**, 2765–2776 (2011), https://doi.org/10.1121/1.3644915.

[9]K.V. Horoshenkov, M.J. Swift, "The acoustic properties of granular materials with pore size distribution close to log-normal," *J. Acoust. Soc. Am.* **110(5)**, 2371–2378 (2001), https://doi.org/10.1121/1.1408312.

[10]P. Glé, E. Gourdon, L. Arnaud, K.V. Horoshenkov, A. Khan, "The effect of particle shape and size distribution on the acoustical properties of mixtures of hemp particles," *J. Acoust. Soc. Am.* **134(6)**, 4698–4709 (2013), https://doi.org/10.1121/1.4824931.

[11]M. Vasina, D.C. Hughes, K.V. Horoshenkov, L. Lapcík Jr., "The acoustical properties of consolidated expanded clay granulates," *Appl. Acoust.* **67**, 787–796 (2006), https://doi.org/10.1016/j.apacoust.2005.08.003.

[12]R. Bartolini, S. Filippozzi, E. Princi, C. Schenone, S. Vicini "Acoustic and mechanical properties of expanded clay granulates consolidated by epoxy resin," *Appl. Clay Sci.* **48(3)**, 460–465 (2010), https://doi.org/10.1016/j.clay.2010.02.007.

[13]Z. Mo, T. Shi, S. Lee, Y. Seo, J.S. Bolton, "A poro-elastic model for activated carbon stacks," *In: Proceedings of the Symposium on the Acoustics of Poro-Elastic Materials (SAPEM) 2021*, online conference, March 2021.

[14]Z. Mazrouei-Sebdani, H. Begum, S. Schoenwald, K.V. Horoshenkov, W.J. Malfait, "A review on silica aerogel-based materials for acoustic applications," *J. Non-Cryst. Sol.* **562**, 120770 (2021), https://doi.org/10.1016/j.jnoncrysol.2021.120770.

[15]A. Ponnappan, A. Choudhary, E. Prasad, “Aerogel Market by Raw Material, Form, and Application: Opportunity Analysis and Industry Forecast, 2020–2027, Allied Market Research,” 2020, www.alliedmarketresearch.com/aerogel-market (last viewed June 6, 2021).

[16]M.M. Koebel, A. Rigacci, P. Achard, “Aerogel-based thermal superinsulation: an overview,” *J. Sol-Gel Sci. Technol.* **63**, 315–339 (2012), https://doi.org/10.1007/s10971-012-2792-9.

[17]J. Fricke, G. Reichenauer, “Thermal Acoustical and structural properties of silica aerogels,” *MRS Proc.* **73**, 73–775 (2011), https://doi.org/10.1557/PROC-73-775.

[18]L. Forest, V. Gibiat, A. Hooley, “Impedance matching and acoustic absorption in granular layers of silica aerogels,” *J. Non-Cryst. Sol.* **285**, 230–235 (2001), https://doi.org/10.1016/S0022-3093(01)00458-6.

[19]H. Begum, K.V. Horoshenkov, M. Conte, W.J. Malfait, S. Zhao, M.M. Koebel, P. Bonfiglio, R. Venegas, “The acoustical properties of tetraethyl orthosilicate based granular silica aerogels,” *J. Acoust. Soc. Am.* **149**, 4149–4158 (2021), https://doi.org/10.1121/10.0005200.

[20]Y. Xue, A. Dasyam, J.S. Bolton, B. Sharma, “Acoustical investigation of aerogel granules modeled as a layer of poro-elastic material,” *In: Proceedings of the Symposium on the Acoustics of Poro-Elastic Materials (SAPEM) 2021*, online conference, March 2021.

[21]K.V. Horoshenkov, K. Attenborough, S.N. Chandler-Wilde, “Pade´ approximants for the acoustical properties of rigid frame porous media with pore size distribution,” *J. Acoust. Soc. Am.* **104**, 1198–1209 (1998), https://doi.org/10.1121/1.424328.

[22]B.H. Song, J.S. Bolton, “A transfer-matrix approach for estimating the characteristic impedance and wave numbers of limp and rigid porous materials,” *J. Acoust. Soc. Am.* **107**, 1131–1152 (2000), https://doi.org/10.1121/1.428404.

[23]ISO10534-2:1998, Acoustics — “Determination of sound absorption coefficient and impedance in impedance tubes — Part 2: Transfer-function method” (International Organisation for Standardization, Geneva, Switzerland, 1998).

[24]P. Glé, E. Gourdon, L. Arnaud, "Acoustical properties of materials made of vegetable particles with severe scales of porosity," *Appl. Acoust.* **72**, 249–259 (2011), https://doi.org/10.1016/j.apacoust.2010.11.003.

[25]Available online at: https://drive.google.com/drive/folders/1avHWRznOymRB5tA0Jx-8x1YcCxD4h-Wc?usp=sharing (Last accessed on July 13, 2021).

[26]H. Begum, K.V. Horoshenkov, "Acoustical Properties of Fiberglass Blankets Impregnated with Silica Aerogel," *Appl. Sci.* **11**, 4593 (2021), https://doi.org/10.3390/app11104593.

[27]MATERIACUSTICA SRL, "Measurement kit for acoustical complex properties testing," https://www.materiacustica.it/mat_UKProdotti_MAA.html (Last viewed January 27, 2021).

[28]D.L. Johnson, J. Koplik, and R. Dashen, "Theory of dynamic permeability and tortuosity in fluid-saturated porous media," *J. Fluid Mech.* **176**, 379–402 (1987), https://doi.org/10.1017/S0022112087000727.

[29]Y. Champoux and J.-F. Allard, "Dynamic tortuosity and bulk modulus in air-saturated porous media," *J. Appl. Phys.* **70(4)**, 1975–1979 (1991), https://doi.org/10.1063/1.349482.

[30]K.V. Horoshenkov, A. Hurrell and J.-P. Groby, "A three-parameter analytical model for the acoustical properties of porous media," J. Acoust. Soc. Am. **145(4)**, 2512–2517 (2019), https://doi.org/10.1121/1.5098778 and https://doi.org/10.1121/10.0000560 (Erratum).

[31]M.A. Biot, "Theory of propagation of elastic waves in a fluid-saturated porous solid," *J. Acoust. Soc. Am.* **28(2)**, 168–191 (1956), https://doi.org/10.1121/1.1908239 and https://doi.org/10.1121/1.1908241.

[32]D. Lafarge, P. Lemarinier, J.-F. Allard, and V. Tarnow, "Dynamic compressibility of air in porous structures at audible frequencies," *J. Acoust. Soc. Am.* **102(4)**, 1995–2006 (1997), https://doi.org/10.1121/1.419690.

[33]Y. Xue, J.S. Bolton and Y. Liu, “Modeling and coupling of acoustical layered systems that consist of elements having different transfer matrix dimensions,” *J. Appl. Phys.* **126**, 165012 (2019), https://doi.org/10.1063/1.5108635.

[34]J.S. Bolton, N.M. Shiau, and Y.J. Kang, “Sound transmission through multi-panel structures lined with elastic porous materials,” *J. Sound Vib.* **191(3)**, 317–347 (1996), https://doi.org/10.1006/jsvi.1996.0125.

[35]L.D. Landau, E.M. Lifshitz, Fluid Mechanics, (2nd ed. Elsevier, Oxford), pp. 89-90, 1987.